BJR

Received: 7 November 2016 | Revised: 12 January 2017 | Accepted: 7 March 2017

https://doi.org/10.1259/bjr.20160859

Cite this article as:
Chawla A, Srinivasan S, Lim T-C, Pulickal GG, Shenoy J, Peh WCG. Dual-energy CT applications in salivary gland lesions. *Br J Radiol* 2017; **90**: 20160859.

REVIEW ARTICLE

Dual-energy CT applications in salivary gland lesions

ASHISH CHAWLA, DABR, SIVASUBRAMANIAN SRINIVASAN, FRCR, TZE-CHWAN LIM, FRCR, GEOIPHY G PULICKAL, FRCR, JAGADISH SHENOY, FRCR and WILFRED C G PEH, FRCR

Department of Diagnostic Radiology, Khoo Teck Puat Hospital, Singapore, Republic of Singapore

Address correspondence to: Dr Ashish Chawla
E-mail: *ashchawla@gmail.com*

ABSTRACT

The increasing availability of dual-energy CT (DECT) has set the stage for an exciting era in CT technology. This technique is extensively used throughout the world with numerous centres working on the applications of DECT in various radiology subspeciality areas. DECT provides many advantages over the conventional single-energy scan. Instead of a single set of images, radiologists have access to multiple sets of images from a single acquisition. The DECT workstation enables the reader to generate images, according to the clinical setting, in order to answer a specific clinical question. Radiologists should be aware of the basic concepts of DECT and the usefulness of each image data set. This article aimed to describe the basic principles, techniques and applications of DECT in the imaging of salivary gland lesions. The specific roles of each image data set, in the context of salivary gland lesions, are also discussed.

INTRODUCTION

In recent years, we bear witness to rapid advancement in CT technology, with the introduction of newer dual-energy (DE) scanners taking the centre stage. Since its availability, DE technology has constantly evolved, with manufacturers exploring new techniques in acquiring DE scans. This has brought dramatic changes in the way such images are acquired, processed and interpreted. Dual-energy CT (DECT) can provide useful information in the evaluation of salivary gland abnormalities, such as sialolithiasis, sialaodenitis, abscesses and benign and malignant tumours.

FUNDAMENTALS OF DUAL-ENERGY CT

The X-ray attenuation property of a material results from Compton scatter and photoelectric effect. These two interactions between the X-ray photons and electrons of the material are essential for the formation of CT images. The probability of these interactions is directly proportional to the atomic number, and in the case of photoelectric effect, it is also dependent on the binding energy of the *k*-shell electron of an atom (*k*-edge). There is more probability of photoelectric effect if the energy of incident photons in X-ray beam is just above the *k*-edge of the material, *i.e.* the material will cause maximum attenuation of the beam and the resultant image will appear hyperdense.

Two main components of the CT machine are the X-ray tube (to generate X-ray photons) and detectors (to detect or record the photons exiting the patient). The incident X-ray beam gets attenuated by the imaged tissues and reaches the detectors after exiting from the patient. The exiting photons convey information about the imaged tissue based on the attenuating property of the tissue. The final CT image that is generated is the expression of attenuation of the incident beam (X-ray photons) by an individual voxel. The attenuation of X-ray beam by a tissue depends upon the material composition of the tissue and the energy of the X-ray beam [kilovoltage (kV) and milliampere second]. Conventional single-energy CT (SECT) utilizes a polychromatic beam of X-rays at a single user-defined energy level. This beam is emitted from a single source (one X-ray tube), with a single type of detector registering and constructing the attenuation map. The contrast difference between various tissues depends on the differences in the attenuation of the three main materials, namely: water in the soft tissue, calcium in bones and iodinated contrast material within the vessels. DECT allows acquisition of attenuation profiles of materials at two energy levels. DECT images are generated at two energy levels—a higher energy level (typically at 140 kV) and a lower energy level (typically at 80 kV or 100 kV). The lower energy levels are obtained at 80 kV for patients weighing $<$80 kg and 100 kV for those weighing $>$80 kg.[1] Mean photon energy of 80 kV and 140 kV beams are 56 keV and 76 keV, respectively. The information obtained at the two energy levels allows differentiation of the three basic materials (water, calcium and iodine) within the voxel. This material decomposition of

Table 1. Dual-energy acquisition methods

Dual-source dual energy	Two tubes and two sets of detectors are placed perpendicular to each other in one gantry with each tube operating independently and simultaneously at two different energy levels. The two sets of detectors register attenuation information separately
Twin beam	Single tube emitting a beam that is pre-filtered widthwise into two halves—low-energy and high-energy components—before traversing the patient. The images are acquired simultaneously by one layer of detectors with half the detectors registering high-energy and the other half absorbing low-energy data
Fast kV switching	Single tube in the gantry emits high- and low-energy beams alternatively in a single gantry rotation. The properties of high-speed sampling detectors are high light output, fast speed and low afterglow
Dual detector	Single tube with two layers of detectors—superficial layer absorbs low-energy spectrum and the deeper layer absorbs high-energy spectrum
Rapid dual rotation	Single tube with two ultrafast sequential rotations, one emitting high-energy beam and subsequent rotation emitting low-energy beam
Photon-counting detector	Single source with novel detectors that can resolve photons at specific energy levels, thus providing information about a voxel at multiple energy levels

kV, kilovoltage.

the tissue is the backbone of DECT technology.[2] DECT is also called "spectral" CT, as it generates images at two spectra of X-rays. Post-processing methods allow subtraction of one material from the data set to generate images without iodinated contrast material [*e.g.* virtual non-contrast (VNC) images] and bone removal images.

METHODS OF DUAL-ENERGY CT ACQUISITION

There are many different techniques used to acquire DE data (Table 1). With the exception of the dual-source DE method, the rest of the techniques utilize a single-source CT system.[1,3] The changes in tube potential are compensated by changes in tube current to enable dose reduction. Although not commercially available at present, the photon-counting detector allows multienergy CT imaging and is predicted to be the future state of CT technology.[4] This method will pave the way for molecular CT and tissue-specific imaging. In this article, we have described the applications of DECT in salivary gland lesions with examples acquired from dual-source DECT scanners.

ADVANTAGES OF DUAL-ENERGY CT

DECT offers numerous advantages over single-energy scan by providing more information about the imaged tissue (Table 2). Multiple data sets of images are generated by DECT from a single-phase examination using various post-processing algorithms.[5] The output of these algorithms produces images that usefully address a specific clinical problem or issue during imaging of salivary glands (Table 3). The images can easily be further manipulated on the workstation, thus providing a robust and comprehensive diagnostic tool for the radiologist. DECT is particularly useful in imaging of the salivary glands, as respiratory motion artefacts and "field of view" limitation of dual-source DECT are not as relevant, compared with body imaging.

APPLICATIONS IN SALIVARY GLAND LESIONS

DECT holds promise for the evaluation of various salivary gland lesions, such as infective/inflammatory lesions, benign tumours and malignant tumours.

Table 2. Image data sets acquired from dual-energy CT (DECT), basic principles and the advantages over single-energy CT (SECT)

Images	Basic principle	Advantages
High-kV and low-kV images	Two sets of information derived from different energy levels; main characteristic of DECT	Provides attenuation value of every voxel at two energy levels
VNC images	Material differentiation property helps in subtracting iodine from the data set	Reduces radiation dose to the patient by avoiding the acquisition of unenhanced images
VMC images	Obtained by extrapolating the DECT data to generate images at specified single-energy levels (range: 40–150 keV)	Helps in metallic artefact reduction and allows lower dose of iodinated contrast material
Weighted average images	Obtained by linear blending of data from two energy levels	The images mimic SECT images and are sent to PACS for interpretation
Iodine overlay images	Colour codes the distribution of iodine within the voxel	Allows objective assessment of contrast enhancement and vascularity
Automated bone removal	Subtraction of calcium from the data set	Quick and accurate bone removal

kV, kilovoltage; PACS, picture archiving and communication system; VMC, virtual monochromatic; VNC, virtual non-contrast.

Table 3. Utility of various dual-energy CT data sets for imaging of the salivary glands

VNC	Identification of sialolithiasis
	Identification of phleboliths in haemangioma
High-kV and high-keV (VMC) images	Evaluation of lesions in the presence of streak artefacts arising from dental implants
Low-kV and low-keV (VMC) images	Visualization of less conspicuous lesion
	Delineation of tumour margins
Iodine overlay images	Objective differentiation of the enhancing solid tumour *vs* solid-cystic lesion *vs* simple cyst
	Assessment of infection, inflammation and abscess
Bone removal images	Evaluation of skull base extension of malignant lesions

kV, kilovoltage; keV, kiloelectron volt; VMC, virtual monochromatic; VNC, virtual non-contrast.

Sialolithiasis and phleboliths

Sialolithiasis presents with intermittent pain as well as swelling and is most commonly associated with the submandibular gland; 85% is in the Wharton's duct, while 15% is in the gland proper.[6] Conventional SECT requires a non-contrast CT examination before a contrast study of the salivary glands to detect salivary gland calculus. However, this increases the overall radiation dose to the patients. The VNC image data set of DECT has been shown to be a reliable alternative to true unenhanced images especially in the kidneys.[7] In thoracic CT, VNC images can identify 85% of calcifications in pulmonary nodules and 97.8% of calcifications in mediastinal lymph nodes.[8] The size and nature of calcifications seen in thoracic CT are similar to sialolithiasis; hence, VNC images can be useful in detecting sialolithiasis (Figure 1). One should keep in mind that the calcifications appear smaller in VNC than in true non-contrast.[8] VNC has only moderate accuracy in detecting calcification in kidneys, and its application for renal calculi is size dependent—being limited for 1–2 mm calculus.[9] This is presumably owing to higher noise in VNC images, part of calcium subtracted as iodine and motion artefacts. Motion blurring is generally not applicable in imaging of the salivary glands, as the neck is not usually susceptible to respiratory motions during scanning. Recognition of phleboliths and distinction from sialolithiasis is essential for the diagnosis of vascular malformation involving the salivary gland.[10] As aforementioned for salivary gland calculus, VNC is also useful in detecting phleboliths, allowing one

Figure 1. Sialolithiasis in a patient with recurrent right submandibular swelling: (a) contrast-enhanced axial CT shows a hyperdense focus (arrow) in the right Wharton duct. (b) Iodine subtraction in the axial virtual non-contrast image confirms a calculus (arrow).

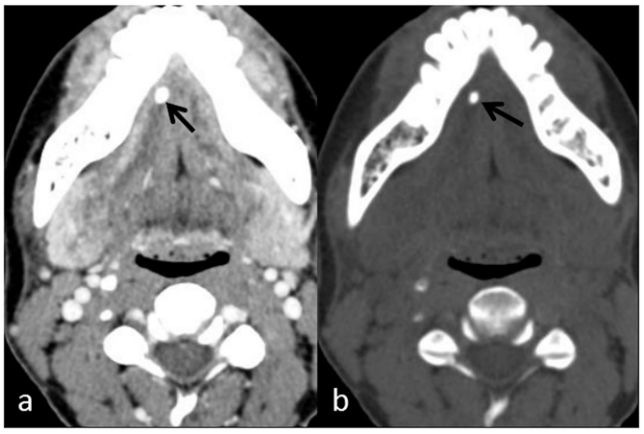

Figure 2. A large facial venous vascular malformation with phleboliths: (a) the coronal contrast-enhanced CT image shows a soft-tissue mass (stars) infiltrating the left submandibular gland. (b) The coronal virtual non-contrast image reveals multiple phleboliths (arrowheads) in the mass, aiding in the diagnosis of a venous vascular malformation.

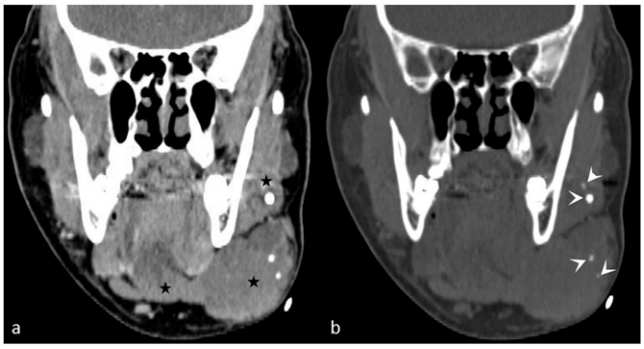

Figure 3. Dual-energy CT of sialadenitis: (a) the axial contrast-enhanced CT image shows asymmetric enlargement of the right submandibular gland (arrow) without any noticeable heterogeneity, with normal size of left submandibular gland (black star). (b) The axial iodine overlay image reveals heterogeneity of iodine distribution with less iodine in the central portion (arrow) of the inflamed right submandibular gland, in addition to its enlargement. The normal left submandibular gland (white star) can be noticed.

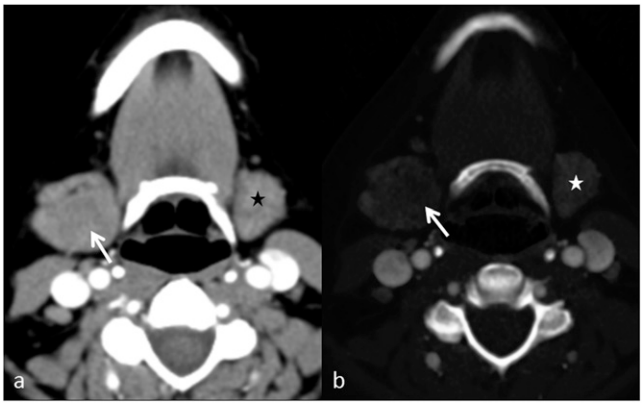

Figure 4. Large parotid abscess: (a) the coronal contrast-enhanced CT image shows a ring enhancing abscess (arrow). (b) The coronal iodine overlay image demonstrates lack of iodine in liquefied portion (arrow), while the vascularized rim and hyperaemic adjacent parenchyma (arrowheads) show iodine uptake.

to diagnose a vascular malformation of the salivary gland (Figure 2). Rarely, pleomorphic adenoma can have focal calcifications that can potentially be detected on VNC images.

Sialadenitis and abscess

The CT features of uncomplicated sialadenitis are asymmetric enlargement of the gland, thickening of overlying facial muscles and stranding of the subcutaneous fat.[11] The scans are frequently normal in early infection or in patients who are intermittently symptomatic. The colour-coded iodine overlay images increase the sensitivity of diagnosing sialadenitis by objective demonstration of the inhomogeneous iodine distribution in early sialadenitis. This is probably owing to interstitial oedema from ongoing inflammation (Figure 3). Abscesses appear on CT as low-attenuating lesions with peripherally enhancing rim of granulation tissue. Iodine overlay images demonstrate the vascularity of the rim as well as reactive hyperaemia (hypervascularity) in the surrounding tissue (Figure 4). The iodine content of the hyperaemic rim can be assessed qualitatively by viewing the monoenergetic images at low energy (such as 50–70 keV) as well as quantitatively, by drawing region of interest circles in the enhancing margins. The enhancement can also be shown by generating virtual monochromatic (VMC) Hounsfield unit curves.[12]

Figure 5. Dual-energy CT in a pleomorphic adenoma: (a) the axial contrast-enhanced CT image shows a subtle mildly enhancing nodule (arrow) in the left parotid gland. (b) The axial iodine overlay image reveals mild iodine uptake in the lesion (arrow), making the lesion more conspicuous.

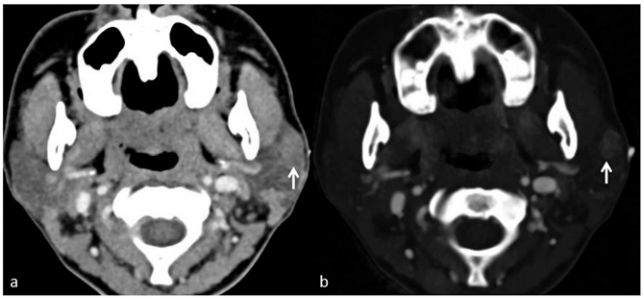

Figure 6. Dual-energy CT in multiple Warthin's tumours: (a) the coronal contrast-enhanced image shows multiple well-circumscribed intensely enhancing nodules in both parotid glands (arrows). (b) The coronal iodine overlay image shows high concentration of iodine in the nodules (arrows).

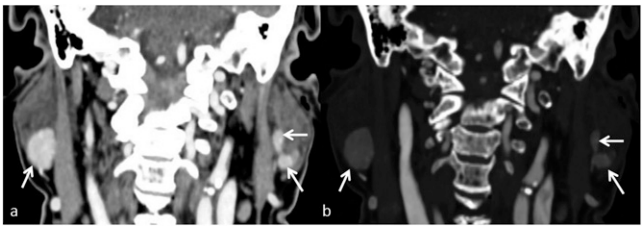

Benign tumours

Enhancement pattern

The three most common benign tumours of the parotid gland are pleomorphic adenoma, Warthin's tumour and lymphoepithelial cyst. Warthin's tumours show early enhancement; pleomorphic adenomas demonstrate delayed enhancement, while lymphoepithelial cysts show no enhancement in dual-phase SECT.[13] Iodine overlay images are valuable in exploiting these enhancement characteristics of benign tumours (Figures 5–7). In a single-phase DECT, pleomorphic adenomas show patchy iodine distribution, while the non-cystic Warthin's tumours show intense iodine uptake. No iodine distribution is seen in a salivary gland cyst. Similarly, a solid-cystic benign tumour, such as Warthin's tumour, shows iodine distribution only in the solid enhancing component. Complete lack of iodine in a non-aggressive lesion of the parotid gland suggests the diagnosis of a cyst, and further confirmatory ultrasound examination may be avoided.

Conspicuity

Benign salivary gland tumours, especially pleomorphic adenomas, may not be appreciated on contrast-enhanced SECT owing to poor enhancement and overall low density of the parotid gland. Similarly, other lesions may also be indistinct in the submandibular gland on SECT.[14] These lesions often require

Figure 7. Dual-energy CT evaluation of a lymphoepithelial cyst: (a) the axial contrast-enhanced image shows a non-enhancing cyst (arrow) in the right parotid gland. (b) The axial iodine overlay image demonstrates lack of iodine in the cyst (arrow).

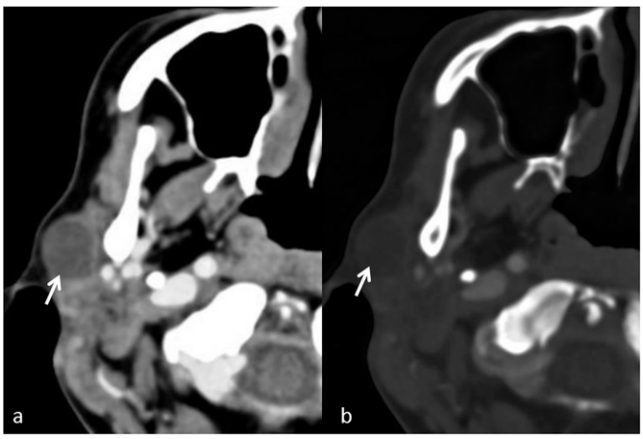

Figure 8. Application of dual-energy CT in improving the conspicuity of a parotid lesion: (a) the axial contrast-enhanced weighted average image shows a subtle lesion (asterisk) expanding the left parotid gland. (b) A low-energy image with better delineation of the margins (arrow) of the lesion.

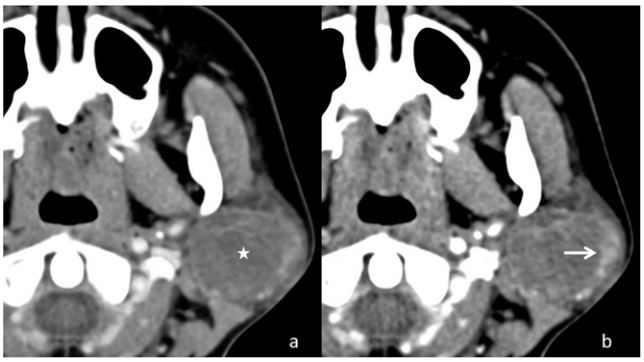

further evaluation with ultrasound and MRI owing to persistent clinical findings.[15] DECT can improve detection of these lesions by utilization of the low-energy (low kV) and low-kiloelectron volt (keV) VMC image data sets. These images improve the conspicuity of indistinct or poorly enhancing lesions owing to the inherent increased sensitivity to contrast (Figures 5 and 8).

Streak artefacts

Metallic dental implants and dental amalgam are very common causes of image degradation in CT of the head and neck. Dental amalgam used for filling up the dental caries is composed of metal.[16] The metallic component absorbs low-energy photons, leading to "hardening" of the beam and producing streak artefacts that appear as dark bands.[17] These streak artefacts often extend to the salivary glands, causing suboptimal or limited evaluation. As these artefacts result from photon starvation (less number of photons reaching the detector), utilization of the high-energy (high kV) data set can help in streak artefact reduction. In addition, the high keV VMC images can also be used to suppress such streak artefacts (Figure 9).[18,19] Bone removal images also aid in detecting the lesion hiding in the streaks (Figure 9).

Figure 9. Usefulness of dual-energy CT in the presence of streak artefacts: (a) the axial contrast-enhanced weighted average image shows asymmetric enlargement of the right parotid gland with suggestion of an enhancing mass (arrow) hidden by the streak artefacts arising from dental prosthesis. (b) The axial high-energy virtual monochromatic (95 keV) image reduces artefacts over the mass, making it more conspicuous. (c) The bone removal image helps by removing the distracting artefacts. The mass was confirmed to be a pleomorphic adenoma.

Contrast dosage

Owing to approximation of the *k*-edge of iodine with the mean photon energy of low-energy beam, the low-energy (low kV) and low-keV VMC image data sets improve the detection of contrast. This has been validated in the evaluation of pulmonary arteries.[20] This important and clinically relevant property of DECT allows the study to be performed with a smaller dose of iodinated contrast. This is particularly useful in patients at risk of contrast-induced nephropathy.

Malignant tumours

Malignant tumours of salivary glands behave in a similar fashion to other malignancies of the head and neck region. The aforementioned applications described for the evaluation of benign tumours are also relevant in the evaluation of malignant lesions.

Figure 10. A left parotid mass with extension in the skull base: (a) the axial contrast-enhanced image shows an enhancing left parotid mass (star) with questionable extension into the left jugular foramen (black arrow). (b) The bone removal image clearly demonstrates the mass in the left parotid (star) with enhancing component in the left jugular foramen (white arrow).

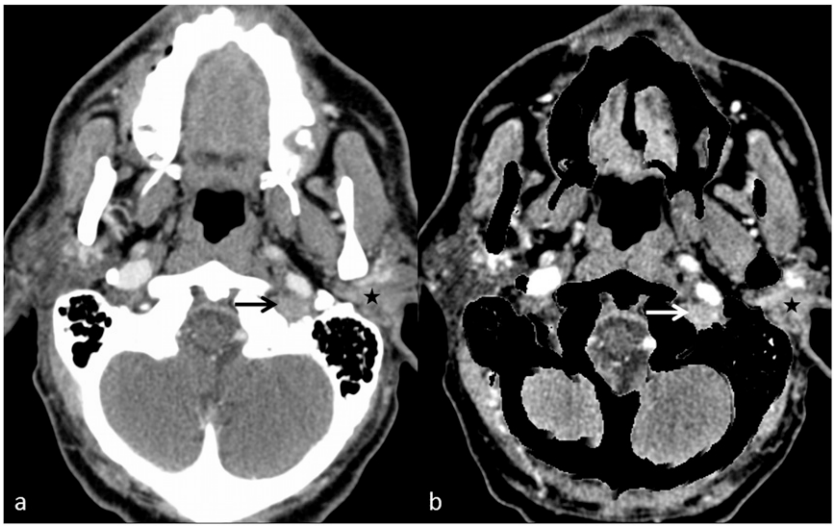

In addition, in our experience, the automated bone removal data set from DECT provides useful information in the assessment of skull base invasion of malignant lesions. Enhancing tumours with intracranial spread *via* the skull base foramina can be better evaluated after subtraction of the bony skull base (Figure 10). DECT is also utilized in radiotherapy treatment planning of head and neck malignancies.[21] VMC at low energy (60 keV) improves the contrast-to-noise ratio and conspicuity of enhancement, hence aiding in better delineation of the malignant tumour.[22] Low-energy data set also provides better assessment of tumour margins in oral cancer.[23,24]

CONCLUSION

CT technology is in the process of transition from attenuation-based imaging of SECT to material-specific imaging of DECT. DECT provides additional information about the tissue composition and, through the various image data sets, offers a more comprehensive imaging approach to the evaluation of salivary gland lesions. To make full use of DECT, one has to appreciate the specific role and utility of each data set. Hence, it is essential for radiologists to understand the basic concepts, techniques and applications of DECT in imaging of the salivary glands.

REFERENCES

1. Johnson TR. Dual-energy CT: general principles. *AJR Am J Roentgenol* 2012; **199**: 3–8. doi: https://doi.org/10.2214/AJR.12.9116
2. Johnson TR, Krauss B, Sedlmair M, Grasruck M, Bruder H, Morhard D, et al. Material differentiation by dual energy CT: initial experience. *Eur Radiol* 2007; **17**: 1510–17. doi: https://doi.org/10.1007/s00330-006-0517-6
3. Lell MM, Wildberger JE, Alkadhi H, Damilakis J, Kachelriess M. Evolution in computed tomography: the battle for speed and dose. *Invest Radiol* 2015; **50**: 629–44. doi: https://doi.org/10.1097/RLI.0000000000000172
4. Taguchi K, Iwanczyk JS. Vision 20/20: single photon counting X-ray detectors in medical imaging. *Med Phys* 2013; **40**: 100901. doi: https://doi.org/10.1118/1.4820371
5. McCollough CH, Leng S, Yu L, Fletcher JG. Dual-and multi-energy CT: principles, technical approaches, and clinical applications. *Radiology* 2015; **276**: 637–53. doi: https://doi.org/10.1148/radiol.2015142631
6. Alyas F, Lewis K, Williams M, Moody AB, Wong KT, Ahuja AT, et al. Diseases of the submandibular gland as demonstrating using high resolution ultrasound. *Br J Radiol* 2005; **78**: 362–9.
7. Takahashi N, Hartman RP, Vrtiska TJ, Kawashima A, Primak AN, Dzyubak OP, et al. Dual-energy CT iodine-subtraction virtual unenhanced technique to detect urinary stones in an iodine-filled collecting system: a phantom study. *AJR Am J Roentgenol* 2008; **190**: 1169–73.
8. Chae EJ, Song JW, Seo JB, Krauss B, Jang YM, Song KS. Clinical utility of dual-energy CT in the evaluation of solitary pulmonary nodules: initial experience. *Radiology* 2008; **249**: 671–81. doi: https://doi.org/10.1148/radiol.2492071956
9. Takahashi N, Vrtiska TJ, Kawashima A. Detectability of urinary stones on virtual nonenhanced images generated at pyelographic-phase dual-energy CT. *Radiology* 2010; **256**: 184–90. doi: https://doi.org/10.1148/radiol.10091411
10. Ho C, Judson BL, Prasad ML. Vascular malformation with phleboliths involving the parotid gland: a case report with a review of the literature. *Ear Nose Throat J* 2015; **94**: 1–5.
11. Yousem DM, Kraut MA, Chalian AA. Major salivary gland imaging. *Radiology* 2000; **216**: 19–29. doi: https://doi.org/10.1148/radiology.216.1.r00jl4519
12. Fulwadhva UP, Wortman JR, Sodickson AD. Use of dual-energy CT and iodine maps in evaluation of bowel disease. *Radiographics* 2016; **36**: 393–406. doi: https://doi.org/10.1148/rg.2016150151
13. Choi DS, Na DG, Byun HS, Ko YH, Kim CK, Cho JM, et al. Salivary gland tumors: evaluation with two-phase helical CT. *Radiology* 2000; **214**: 231–6. doi: https://doi.org/10.1148/radiology.214.1.r00ja05231
14. Kei PL, Tan TY. CT "invisible" lesion of the major salivary glands a diagnostic pitfall of contrast-enhanced CT. *Clin Radiol* 2009; **64**: 744–6.
15. Thomas R, Burke C, Howlett D. Re: CT "invisible" lesion of the major salivary glands-a diagnostic pitfall of contrast-enhanced CT. *Clin Radiol* 2009; **64**: 1137.
16. Scheinfeld MH, Shifteh K, Avery LL, Dym H, Dym RJ. Teeth: what radiologists should know. *Radiographics* 2012; **32**: 1927–44. doi: https://doi.org/10.1148/rg.327125717
17. Barrett JF, Keat N. Artifacts in CT: recognition and avoidance. *Radiographics* 2004; **24**: 1679–91. doi: https://doi.org/10.1148/rg.246045065
18. Bamberg F, Dierks A, Nikolaou K, Reiser MF, Becker CR, Johnson TR. Metal artifact reduction by dual energy computed tomography using monoenergetic extrapolation. *Eur Radiol* 2011; **21**: 1424–9. doi: https://doi.org/10.1007/s00330-011-2062-1
19. Zhou C, Zhao YE, Luo S, Shi H, Zheng L, Zhang LJ, et al. Monoenergetic imaging of dual-energy CT reduces artifacts from implanted metal orthopedic devices in patients with factures. *Acad Radiol* 2011; **18**: 1252–7.
20. Gorgos A, Remy-Jardin M, Duhamel A, Faivre JB, Tacelli N, Delannoy V, et al. Evaluation of peripheral pulmonary arteries at 80 kV and at 140 kV: dual-energy computed tomography assessment in 51 patients. *J Comput Assist Tomogr* 2009; **33**: 981–6.
21. van Elmpt W, Landry G, Das M, Verhaegen F. Dual energy CT in radiotherapy: current applications and future outlook. *Radiother Oncol* 2016; **119**: 137–44. doi: https://doi.org/10.1016/j.radonc.2016.02.026
22. Wichmann JL, Nöske EM, Kraft J, Burck I, Wagenblast J, Eckardt A, et al. Virtual monoenergetic dual-energy computed tomography: optimization of kiloelectron volt settings in head and neck cancer. *Invest Radiol* 2014; **49**: 735–41. doi: https://doi.org/10.1097/rli.0000000000000077
23. Toepker M, Czerny C, Ringl H, Fruehwald-Pallamar J, Wolf F, Weber M, et al. Can dual-energy CT improve the assessment of tumor margins in oral cancer? *Oral Oncol* 2014; **50**: 221–7. doi: https://doi.org/10.1016/j.oraloncology.2013.12.001
24. Vogl TJ, Schulz B, Bauer RW, Stöver T, Sader R, Tawfik AM. Dual-energy CT applications in head and neck imaging. *AJR Am J Roentgenol* 2012; **199**: 34–9. doi: https://doi.org/10.2214/AJR.12.9113